Journal of Zhejiang University-SCIENCE B (Biomedicine & Biotechnology) *2023 24(9):807-822*
www.jzus.zju.edu.cn; www.springer.com/journal/11585
E-mail: jzus_b@zju.edu.cn

Research Article

https://doi.org/10.1631/jzus.B2200692

Genetic and histological relationship between pheromone-secreting tissues of the musk gland and skin of juvenile Chinese forest musk deer (*Moschus berezovskii* Flerov, 1929)

Long LI[1*], Heran CAO[1,3*], Jinmeng YANG[1], Tianqi JIN[1], Yuxuan MA[1], Yang WANG[1], Zhenpeng LI[1], Yining CHEN[1], Huihui GAO[1], Chao ZHU[1], Tianhao YANG[1], Yalong DENG[1], Fangxia YANG[2,3✉], Wuzi DONG[1,3✉]

[1]*College of Animal Science and Technology, Northwest A&F University, Yangling 712100, China*
[2]*College of Forestry, Northwest A&F University, Yangling 712100, China*
[3]*Biology Research Centre of Qin Mountains Wildlife, Northwest A&F University, Yangling 712100, China*

Abstract: Background: The musk glands of adult male Chinese forest musk deer (*Moschus berezovskii* Flerov, 1929) (FMD), which are considered as special skin glands, secrete a mixture of sebum, lipids, and proteins into the musk pod. Together, these components form musk, which plays an important role in attracting females during the breeding season. However, the relationship between the musk glands and skin of Chinese FMD remains undiscovered. Here, the musk gland and skin of Chinese FMD were examined using histological analysis and RNA sequencing (RNA-seq), and the expression of key regulatory genes was evaluated to determine whether the musk gland is derived from the skin. Methods: A comparative analysis of musk gland anatomy between juvenile and adult Chinese FMD was conducted. Then, based on the anatomical structure of the musk gland, skin tissues from the abdomen and back as well as musk gland tissues were obtained from three juvenile FMD. These tissues were used for RNA-seq, hematoxylin-eosin (HE) staining, immunohistochemistry (IHC), western blot (WB), and quantitative real-time polymerase chain reaction (qRT-PCR) experiments. Results: Anatomical analysis showed that only adult male FMD had a complete glandular organ and musk pod, while juvenile FMD did not have any well-developed musk pods. Transcriptomic data revealed that 88.24% of genes were co-expressed in the skin and musk gland tissues. Kyoto Encyclopedia of Genes and Genomes (KEGG) signaling pathway analysis found that the genes co-expressed in the abdomen skin, back skin, and musk gland were enriched in biological development, endocrine system, lipid metabolism, and other pathways. Gene Ontology (GO) enrichment analysis indicated that the genes expressed in these tissues were enriched in biological processes such as multicellular development and cell division. Moreover, the Metascape predictive analysis tool demonstrated that genes expressed in musk glands were skin tissue-specific. qRT-PCR and WB revealed that sex-determining region Y-box protein 9 (*Sox9*), Caveolin-1 (*Cav-1*), and androgen receptor (*AR*) were expressed in all three tissues, although the expression levels differed among the tissues. According to the IHC results, Sox9 and AR were expressed in the nuclei of sebaceous gland, hair follicle, and musk gland cells, whereas Cav-1 was expressed in the cell membrane. Conclusions: The musk gland of Chinese FMD may be a derivative of skin tissue, and Sox9, Cav-1, and AR may play significant roles in musk gland development.

Key words: Forest musk deer; Pheromones; Musk gland; Skin tissues; Transcriptome; Sebaceous gland

1 Introduction

Pheromone secretion is a key function of the skin, which has three main types of accessory structures (sebaceous glands, eccrine sweat glands, and hair follicles), all of which are derived from the developing epidermis (Saga, 2002; Sotiropoulou and Blanpain, 2012; Biggs and Mikkola, 2014; Fuchs, 2016). Unlike "animal scent signatures" that consist of complex and variable mixtures of scent molecules, mammalian pheromones induce function- and species-specific responses (Shirasu

✉ Wuzi DONG, dongwuzi@nwsuaf.edu.cn
Fangxia YANG, yangfangxia@nwsuaf.edu.cn
* The two authors contributed equally to this work
Wuzi DONG, https://orcid.org/0000-0001-6023-2899
Fangxia YANG, https://orcid.org/0009-0005-2361-0711
Long LI, https://orcid.org/0000-0001-9484-8579

Received Dec. 28, 2022; Revision accepted Mar. 23, 2023; Crosschecked Aug. 11, 2023

et al., 2020). Animals synthesize and release pheromones into their environment to communicate with other members of the same species. Hence, pheromones have been extensively studied in mammals, including humans (Varendi and Porter, 2001; Slessor et al., 2005).

In the Chinese forest musk deer (*Moschus berezovskii* Flerov, 1929) (FMD), musk secretion is important for breeding, territory identification, and recovery from disease. The main factor regulating the secretion of musk in adult males is the level of androgens (Yang et al., 2021; Jiang et al., 2022). The musk gland is an exocrine gland, which can only secrete musk in sexually mature male FMD (Sokolov et al., 1987). The epithelial cells of musk glands secrete musk in an apocrine manner, and the musk enters the musk pod via a duct (Chen et al., 2018).

The skin of animals is a complex organ with many accessory tissues that perform unique functions in different parts of the body. Sebaceous glands in the skin are necessary for its development and homeostasis (Picardo et al., 2015). In FMD, the sebum secreted by sebaceous glands in the neck and the ducts of the bursa enters the musk pod. Here, the immature musk and sebum gradually mature for about two months (Chen et al., 2018; Lv et al., 2022). Most sebaceous glands are associated with hair follicles and form follicular sebaceous gland units that produce sebum following the differentiation and disintegration of fully mature sebaceous cells (Thody and Shuster, 1989; Downie et al., 2004; Smith and Thiboutot, 2008; Zouboulis et al., 2008; Schneider and Paus, 2010). Sex-determining region Y-box protein 9 (Sox9) is expressed in keratinocytes, sebaceous glands, sweat glands, and melanocytes (Vidal et al., 2008; Shi et al., 2013; Shakhova et al., 2015). *Sox9* can promote proliferation, differentiation, and sebum secretion by sebaceous gland cells (Shi et al., 2017). It is also essential for the development of skin tissue, plays a role in regulating hair follicle stem cell differentiation, and is necessary for the morphogenesis of hair follicles and sebaceous glands (Smith and Thiboutot, 2008; Shakhova et al., 2015; Shi et al., 2017). Caveolin-1 (*Cav-1*) is highly expressed in several cells and can interact with multiple proteins, serving as a signal transduction hub of cell signaling molecules (Boscher and Nabi, 2012; Fridolfsson et al., 2014). Studies have shown that Cav-1 can promote cell differentiation in a specific direction in a variety of cell types (Fu et al., 2012; Codenotti et al., 2016). Furthermore, it plays an important role in regulating lipid metabolism, especially in adipose tissue (Bastiani et al., 2009). Meanwhile, the androgen receptor (AR) protein, an important member of the steroid receptor superfamily, is expressed in many skin cells such as hair follicles, sebaceous glands, and sweat glands (Fu et al., 2012; Codenotti et al., 2016). The secretion of sebum is closely related to the function of sebaceous glands, and androgens, especially dihydrotestosterone, regulate this function through ARs (Huang et al., 2018; Duarte et al., 2019). The Sox9/AR/Wnt/β-catenin signaling pathway can activate target genes responsible for cell viability, proliferation, and differentiation (Khurana and Sikka, 2019). The palmitoylation of cysteine residues in Cav-1 promotes its binding to AR. Testosterone induces the binding of AR to Cav-1 and its localization to the cell membrane (Bennett et al., 2009). Therefore, *Sox9*, *Cav-1*, and *AR* could be potentially involved in regulating the development of skin and gland tissues as well as musk secretion in FMD.

However, the relationship between the skin tissue and musk gland of Chinese FMD, as well as the expression of regulatory genes in these tissues, remains to be elucidated. To clarify the relationship between the skin tissue and musk gland during the developmental period, we dissected tissue from male FMD of different ages (four months of age and adulthood) and selected the developing 4-month-old FMD as our research model. RNA sequencing (RNA-seq), immunohistochemistry (IHC), western blot (WB), and quantitative real-time polymerase chain reaction (qRT-PCR) were used to examine the musk gland, abdomen skin, and back skin of 4-month-old FMD specimens.

2 Materials and methods

2.1 Anatomical comparison

Chinese FMD who died accidentally (from accidents or fights) at farms (Shaanxi Baosen Musk Deer Industry, China) were chosen for this study. Based on age determination, we classified three FMD as juveniles (4-month-old, before sexual maturity) and three as adults (6-year-old, after sexual maturity). The carcasses of FMD from these two groups were dissected, and the structures of the musk gland and skin tissue were compared.

2.2 Tissue sample collection and cryopreservation

The carcasses of experimental animals were collected according to the guidelines of the ethics committee. Immediately after death, the FMD were transferred to the laboratory, and the back skin, abdominal skin, and musk gland were isolated. Additionally, musk gland and skin tissues were collected for IHC, WB, and transcriptome sequencing. Samples for hematoxylin-eosin (HE) staining and IHC were trimmed into approximately 1 cm^3 pieces and subsequently fixed with 4% (volume ratio) paraformaldehyde. The samples were washed with phosphate-buffered saline (PBS), immediately transferred to a new RNase-free tube, and stored in a −80 ℃ refrigerator until the extraction of total RNA and protein content.

2.3 Total RNA extraction and cDNA synthesis

The total RNA was extracted from each tissue using the TRIzol reagent (Invitrogen, CA, USA). A Nanodrop 2000 spectrophotometer (ThermoFisher Scientific, DE, USA) was utilized for testing the RNA concentration and purity (the ratio of optical density at 260 nm (OD_{260}) to OD_{280} is >1.8), and 1 μg of good-quality RNA was reverse-transcribed using a complementary DNA (cDNA) synthesis kit (Code No. 6110A, TaKaRa, Japan) for qRT-PCR. All experimental steps were performed according to the manufacturer's instructions.

2.4 Total RNA extraction and RNA-seq

Total RNA was extracted from abdominal skin, back skin, and musk gland tissues using the TRIzol reagent. The purity and content of total RNA were quantified using a Bioanalyzer 2100 Spectrophotometer (Agilent, CA, USA) and RNA 1000 Nano LabChip Kit (Agilent). Total RNA was used for subsequent experiments if the samples met the following criteria: RNA 28S:RNA 18S is ⩾1.5 and RNA integrity number (RIN) is ⩾7.0. RNA-seq and sequencing library preparation were performed by Lianchuan Biotech (Hangzhou, China).

2.5 RNA-seq bioinformatics analysis

Low-quality information from the sequenced data was filtered using SOAPnuke (v1.5.2; SOAPnuke, Research Resource Identifier (RRID): SCR_015025) (Li et al., 2008). To evaluate sequence quality, the Q20 (Phred quality score threshold of 20), Q30 (Phred quality score threshold of 30), and guanine-cytosine (GC) content of the clean data were evaluated (Andrews, 2014). The Trinity (Version 2.4.0; Trinity, Broad Institute) (Haas et al., 2013) tool was used for transcriptome de novo assembly. After assembly, TransDecoder (Version 3.0.1; http://transdecoder.github.io) was employed to predict the coding domain sequences (CDSs). To obtain high-quality non-redundant CDSs, encoding sequences with less than 100 amino acids were removed, and the assembled unigene data were annotated against the non-redundant protein database (https://ftp.ncbi.nlm.nih.gov/blast/db), the Gene Ontology (GO) database for functional enrichment analysis (http://geneontology.org), the Pfam database (https://pfam.xfam.org), the Kyoto Encyclopedia of Genes and Genomes (KEGG) database for signaling pathway analysis (https://www.genome.jp/kegg), the SwissProt database (https://www.uniprot.org), and the eggNOG database (http://eggnogdb.embl.de) by applying DIAMOND (Version 0.7.12) and a threshold of E-value$<1\times10^{-5}$ (Buchfink et al., 2015).

2.6 Gene quantification by qRT-PCR

The messenger RNA (mRNA) expression levels of candidate genes were detected by qRT-PCR using SYBR Green I (AceQ qPCR SYBR Green Master Mix, Vazyme Biotech, Nanjing, China). The qRT-PCR protocol was carried out in a 96-well plate, and glyceraldehyde-3-phosphate dehydrogenase (*GAPDH*) was used as the endogenous reference gene. Specific primers designed using Primer Premier 6.0 (Premier Biosoft, CA, USA) and synthesized by Tsingke Biotech (Beijing, China) were used to amplify the candidate genes. The primer sequences are shown in Table 1. The qRT-PCR amplification conditions included an initial denaturation step of 5 min at 95 ℃, followed by 40 cycles of denaturation at 95 ℃ for 10 s, annealing at 60 ℃ for 30 s, and extension at 72 ℃ for 10 s. The melt curve required an additional heating step at 95 ℃ for 15 s, 60 ℃ for 60 s, and 95 ℃ for 15 s. Comparative threshold cycles were calculated for each target gene. *GAPDH* expression levels were used for normalization, and the target gene expression was calculated using the $2^{-\Delta\Delta C_T}$ method.

2.7 HE staining and immunohistochemistry

The abdominal skin, back skin, and musk glands of FMD were fixed in 4% paraformaldehyde, then

Table 1 Primer sequences used for qRT-PCR

Gene symbol	Sense (5'→3')	Antisense (5'→3')	Product length (bp)
Sox9	GCAGTACGACTACAGCGACC	TGAAGGTGGAGTAGAGGCCG	86
Cav-1	CCAAGCATCTCAACGACGA	AAGAGGGCAGACAGCAAACG	155
AR	CCCCATTCGGCTACACTCG	GATAGGGCACTCTGCTCACCAC	108
GAPDH	CGACAAGTATAACAACACCCTC	GTCATAAGTCCCTCCACGAT	117

AR: androgen receptor; *Cav-1*: Caveolin-1; *GAPDH*: glyceraldehyde-3-phosphate dehydrogenase; qRT-PCR: quantitative real-time polymerase chain reaction; *Sox9*: sex-determining region Y-box protein 9.

dehydrated and cleared with xylene until tissue became transparent, and finally embedded in paraffin. All paraffin blocks were cut into 5-μm thick sections, which were mounted on slides. Some of these tissue sections were used for HE staining, and the rest were utilized for IHC.

In brief, the protocol of HE staining mainly included deparaffinization, rehydration, hematoxylin staining, and eosin staining. The tissue morphology was observed under a microscope (Nikon Ni-U, Japan) after sealing. The IHC method was used to identify Sox9, Cav-1, and AR localization in the back skin, abdominal skin, and musk glandular tissue. Dewaxing, rehydration, permeation, and antigen retrieval were the main initial steps of the IHC experimental procedure. Next, the tissues were incubated in 3% (volume ratio) hydrogen peroxide (H_2O_2) for 10 min to block any endogenous hydroperoxide activity. Subsequently, the tissues were blocked with 5% (volume ratio) bovine serum albumin (BSA) for 2 h and then washed with PBS three times (5 min per wash). Primary antibodies against Sox9 (1:200 (volume ratio, the same below); Cat. No. ab185966; Abcam, Cambridge, UK), Cav-1 (1:100; Cat. No. sc-53564; Santa Cruz Biotechnology, Santa Cruz, CA, USA), and AR (1:100; Cat. No. sc-7305; Santa Cruz Biotechnology) were diluted using Dako Antibody Diluent (Code S2022, Agilent, CA, USA). Tissue sections were incubated with the primary antibodies overnight at 4 ℃. Next, the tissues were washed, and secondary antibody labeling was performed by incubating tissues with the secondary antibody for 1 h at 25 ℃ according to the protocol of the SPlink Detection Kit (Zsbio Commerce Store, Beijing, China). Finally, after 3,3'-diaminobenzidine (DAB) staining, tissue sections were kept in the dark for 5 min and counterstained with hematoxylin reagent for 3 min.

2.8 Western blot analysis

Total tissue protein was extracted from the back skin, abdominal skin, and musk gland. All tissues were homogenized in radio immunoprecipitation assay (RIPA) lysis solution (RIPA:phenylmethanesulfonyl fluoride (PMSF)=100:1 (volume ratio); Beyotime Biotechnology, Shanghai, China) using a high-speed homogenizer. The homogenates were incubated on ice for 20 min, and then centrifuged at 13 400 r/min for 10 min at 4 ℃. Approximately 75% (volume ratio) of the RIPA buffer volume was collected as supernatant and thoroughly mixed with an equal volume of 2× Laemmli sample buffer. The total protein concentration in each sample was detected using the BCA Assay Kit (Pierce, Rockford, IL, USA). Equal amounts of proteins were added to each lane of a 12% (volume ratio) sodium dodecyl sulfate-polyacrylamide gel electrophoresis (SDS-PAGE) gel and electrophoresed at 18 V/cm to separate the total proteins. The separated proteins were transferred onto polyvinylidene difluoride (PVDF) membranes using a semi-dry transfer device (Bio-Rad, CA, USA). The membranes were collected and blocked with 5% BSA for 1 h at 25 ℃, and then incubated overnight with primary antibodies at 4 ℃ on a shaker. The antibody dilutions used were as follows: Sox9 (1:1000), Cav-1 (1:500), and AR (1:500). The target proteins were detected with the corresponding secondary antibodies after incubating the membrane for 1 h at 25 ℃. Finally, the expression of the target protein was normalized based on that of endogenous β-actin and calculated by computing the ratio of target protein expression to β-actin expression.

2.9 Statistical analysis

For all statistical analyses performed in this study, GraphPad Prism (Version 8.0) software was used. Data were expressed as mean±standard deviation (SD), and an unpaired *t*-test was used for statistical comparison. Significance values were expressed as * $P<0.05$, ** $P<0.01$, *** $P<0.001$, and not significant (ns). R software was implemented to prepare a Venn diagram of genes expressed in the abdominal skin, back skin, and musk glands.

3 Results

3.1 Anatomical analysis

By dissecting the musk gland tissue of Chinese FMD at different stages, we found that at four months of age (Fig. S1a), the musk gland had already started developing. However, the musk pod was only present in 6-year old adult male FMD (Fig. S1b). The tissue anatomy was compared between the musk glands of developing and adult male FMD. To further study the relationship between the skin and the musk gland, juvenile FMD (4-month-old) were selected as the research model.

3.2 Quality control for transcriptome sequencing data

The transcriptome sequencing results for the musk gland, back skin, and abdominal skin are shown in Table 2. The Q20, Q30, and GC percentages can reflect the quality of clean reads. The Q20 values of the musk gland and skin tissue sequencing data reached over 97%, and the Q30 values were over 93%. This showed that the sequencing process was accurate, and the data came from high-quality sources. The length distribution of assembled unigenes is shown in Fig. 1. Most genes were in the 200–300 bp or ≥2000 bp range. The assembled gene sequences were considered transcripts and used for further analysis.

3.3 Differential expression of expressed genes

The numbers of genes co-expressed and specifically expressed in the back skin, abdominal skin, and musk glands were visualized using Venn diagrams (Fig. 2). The vast majority of genes (29 771) were expressed in all three tissues, accounting for 88.24% of all predicted genes. Only a few genes showed tissue

Table 2 Overview of quality control for transcriptome sequencing data

Sample	Raw reads	Raw bases ($\times 10^9$ bp)	Valid reads	Valid bases ($\times 10^9$ bp)	Valid (%)	Q20 (%)	Q30 (%)	GC (%)
Musk	55 237 098	8.29	53 488 432	7.48	96.83	98.33	94.54	49.15
Abdomen skin	54 709 886	8.21	49 022 732	6.68	89.60	97.76	93.18	50.82
Back skin	46 598 196	6.99	44 357 912	6.04	95.19	97.74	93.10	47.91

Q20: Phred quality score threshold of 20; Q30: Phred quality score threshold of 30; GC: guanine-cytosine.

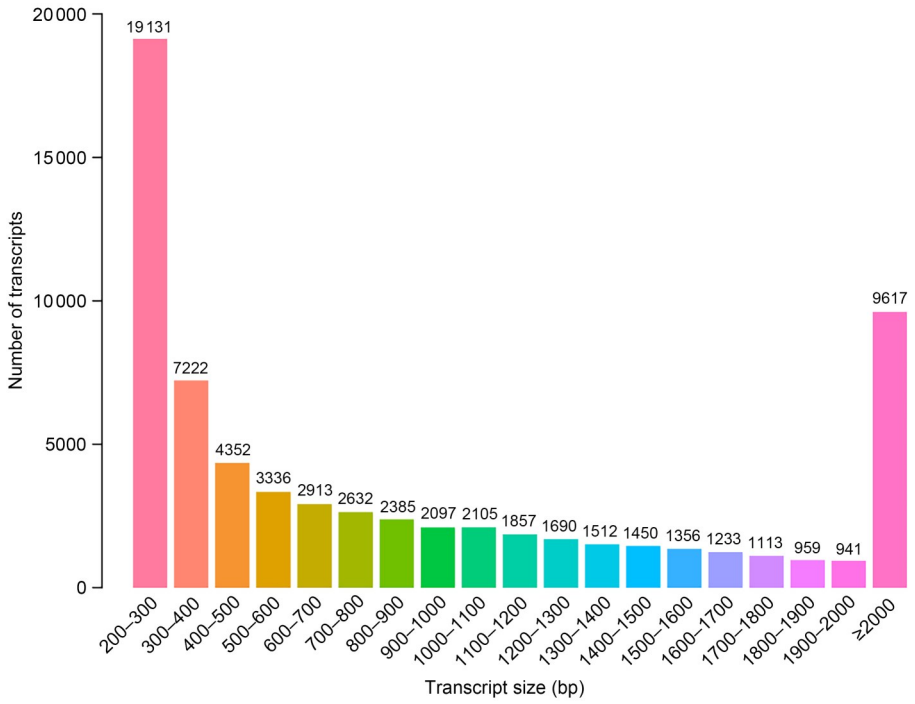

Fig. 1 Unigene length distribution in forest musk deer (FMD). The *x*-axis indicates the length of sequenced unigenes and the *y*-axis indicates the number of sequenced unigenes.

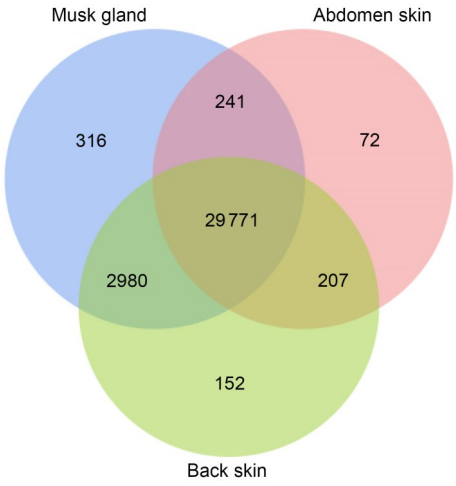

Fig. 2 Venn diagram indicating gene expression (transcriptome datasets) in the back skin, abdominal skin, and musk gland tissue of forest musk deer (FMD). The overlapping sections indicate the genes co-expressed in different tissues.

specificity, which indicated that the musk glands, abdominal skin, and back skin had a high degree of similarity at the genetic level. Using a TPM (transcripts per million tags) threshold of 25, 2866 genes from the musk gland transcriptome were screened. With human genes as the reference gene set, the gene enrichment analysis software Metascape (https://metascape.org/gp/index.html#/main/step1) was employed to analyze the cell and tissue specificity of genes in the musk gland tissue (Zhou et al., 2019). The Metascape analysis revealed that these genes were significantly enriched in skin tissues (Fig. 3). We analyzed the abdominal skin and back skin transcriptomes using the same screening criteria described above. The same results were obtained, i.e., these genes were enriched in adipocytes, bronchial epithelial cells, and skin tissue (Fig. S2). These data indicated a strong relationship between musk gland tissue and skin tissue.

3.4 Functional annotation of the transcriptome

The GO database, established by the Gene Ontology Consortium, contains a large amount of information on gene function. Using this database, genes and gene products can be annotated into three categories: biological process, molecular function, and cellular component. In this study, GO enrichment analysis of differentially expressed genes in the back skin, abdominal skin, and musk gland tissue was performed. With $P<0.05$ as a screening condition, the entries with the highest significance in each group and each category of GO enrichment were presented (Fig. 4). In the musk gland vs. back skin group, 2803 genes were significantly enriched across 621 available GO terms: 155 were enriched in the molecular function module, 393 in the biological process module, and 73 in the cellular component module. We identified significantly enriched pathways for the structural constituents of muscle, focal adhesion, and adenylate cyclase-inhibiting dopamine receptor. In addition, entries related to skin development and differentiation, endodermal cell differentiation and sebaceous gland cell differentiation were also observed (Fig. S3a). The analysis of genes differentially expressed in the musk gland and abdominal skin revealed 4911 genes that were significantly enriched for 469 available GO terms. Of these, 79 were enriched in the molecular function module, 316 in the biological process module, and 74 in the cellular component module. The most significant enrichment was observed for the following categories: structural molecule activity, establishment of protein localization, and extracellular exosomes. In addition, functions related to endodermal

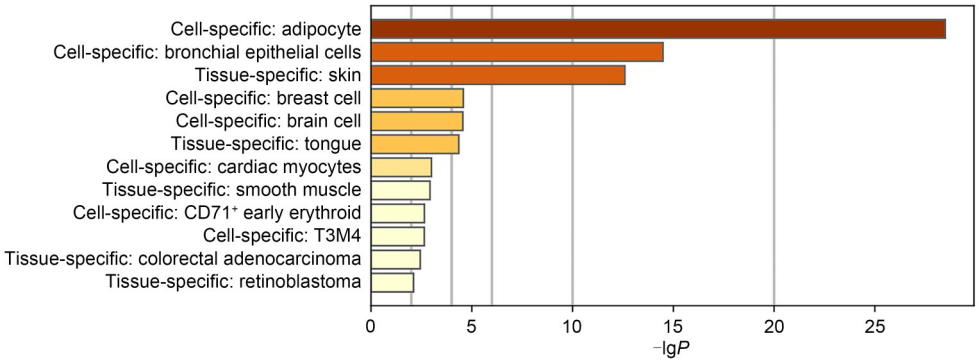

Fig. 3 Gene Metascape enrichment in forest musk deer (FMD) musk gland tissues. The Metascape software was used to analyze gene specificity in tissue and cells.

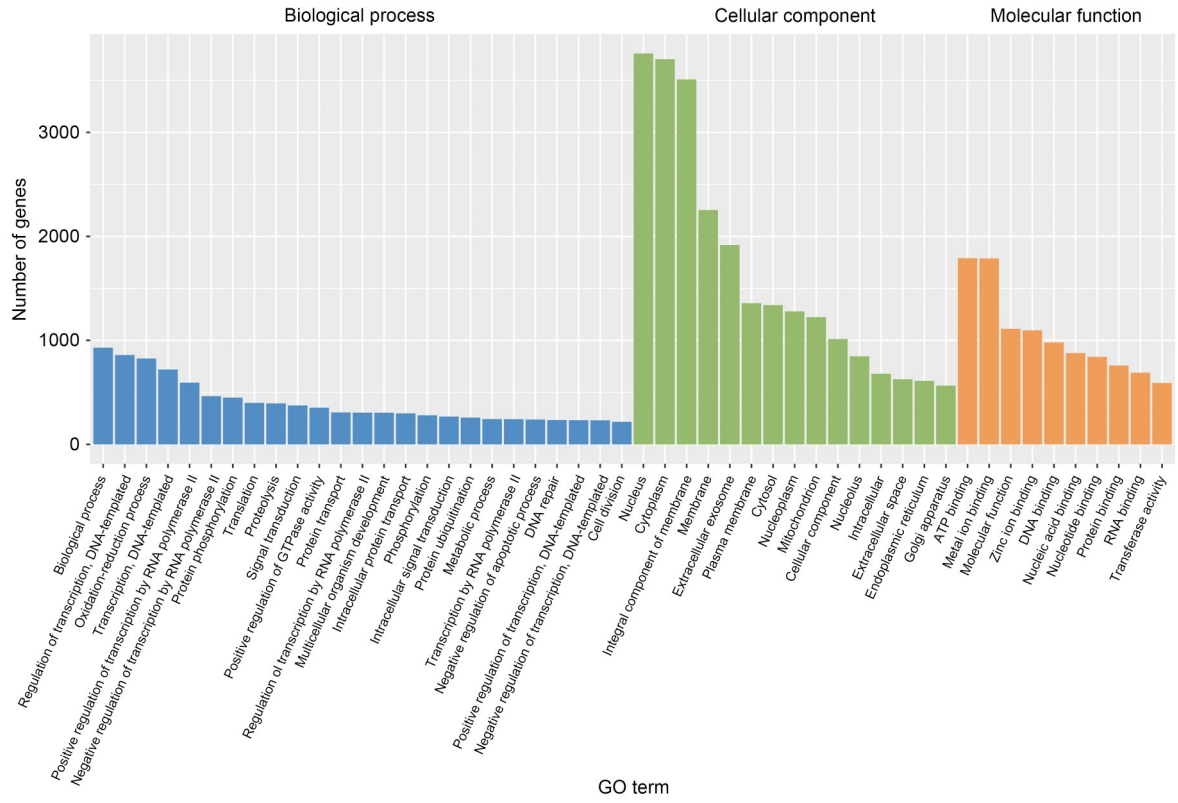

Fig. 4 Gene Ontology (GO) functional classification of co-expressed genes. The GO database allows for the annotation of genes and gene products across three categories: biological process, molecular function, and cellular component.

cell differentiation and cytokine secretion were identified (Fig. S3b). In the analysis of genes differentially expressed in the back skin vs. abdominal skin, 4435 genes were found to be significantly enriched for 414 available GO entries: 90 in the molecular function module, 263 in the biological process module, and 61 in the cellular component module (Fig. S3c).

3.5 KEGG signaling pathway prediction

We performed experimental KEGG pathway analysis to further identify the functional pathways involving the genes co-expressed in the abdominal skin, back skin, and musk glands. The signaling pathways predicted based on transcriptome data were divided into six main categories: organismal systems, metabolism, human diseases, genetic information processing, environmental information processing, and cellular processes (Fig. 5). A total of 1195 genes were significantly enriched in 99 KEGG metabolic pathways according to the comparative analysis of musk glands and back skin. The top three pathways with the most significant enrichment were fat digestion and absorption, glycerolipid metabolism, and estrogen signaling pathway (Fig. S4a). A total of 1612 genes were significantly enriched for 55 KEGG metabolic pathways in the comparative analysis of musk gland and abdominal skin, with the top three pathways with the highest significance being thermogenesis, Alzheimer's disease, and ribosome (Fig. S4b). In total, 1795 genes were significantly enriched for 68 KEGG metabolic pathways in the comparative analysis of back skin vs. abdominal skin (Fig. S4c). The top three significantly enriched pathways were thermogenesis, estrogen signaling pathway, and Huntington's disease.

3.6 Tissue HE staining

The cellular structure of different tissues in musk glands can be visualized using HE tissue staining. The musk gland of FMD has multiple parts, including lax connective tissue, distributed sebaceous glands, the musk gland part, and the acinar cavity (Fig. 6a). HE staining of the skin and hair follicles at the musk gland–skin junction revealed an intact hair follicle structure and abundant sebocytes (Fig. 6b). In the musk glandular region, a large number of ACs were detected (Fig. 6c).

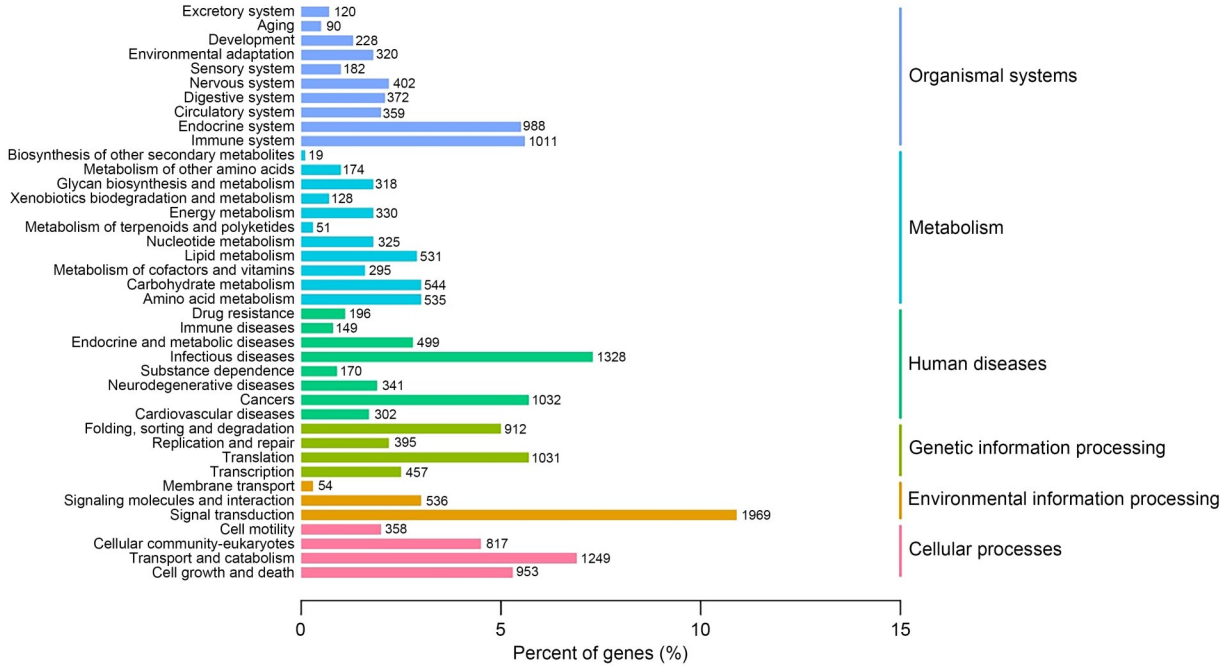

Fig. 5 Histogram illustrating the Kyoto Encyclopedia of Genes and Genome (KEGG) pathway classification of genes co-expressed in the abdominal skin, back skin, and musk gland tissues. The *x*-axis indicates the percentage of genes annotated to a pathway. The *y*-axis indicates the KEGG pathways, with different colors corresponding to the six categories in the top layer.

In order to further study the skin tissue, sections of skin tissues were stained using HE. The structure of the skin tissue was examined. We found that the innermost layer was composed of muscle tissue, followed by adipose tissue, subcutaneous tissue, and the epidermal layer (Fig. 6d). The section of the skin and hair follicles revealed that the hair follicles surrounded by sebaceous glands at different stages of development were different: in the early stage of development, the number of sebocytes was high, but the hair follicle space was small. Meanwhile, well-developed hair follicles had few sebocytes around them, and the space around the hair follicles was large (Fig. 6e). The complete section of a hair follicle was analyzed and found to contain a hair shaft cuticle, hair shaft cortex, and hair shaft medulla (Fig. 6f).

Given that hair follicles have different degrees of sebocyte encapsulations at different developmental stages, we conducted an in-depth study of the skin–hair follicle junction. The sections of the skin–follicle junction were obtained and stained with HE. The results showed that sebaceous glands and hair follicles may act as a structural unit, including hair follicles, sebaceous glands, and hair shafts (Fig. 6g), and the hair follicle is surrounded by a large number of sebaceous cells (marked by black arrows in Fig. 6h). HE staining revealed a complete hair shaft structure (Fig. 6i), with the hair shaft medulla forming the innermost structure, followed by the hair shaft cortex and cuticle.

3.7 Immunohistochemistry

Immunohistochemical staining revealed the localization of Sox9, Cav-1, and AR proteins in the abdominal skin, back skin, and musk gland tissues. In the negative control, the nuclei were light blue in color, and the cytoplasm and background were colorless (Figs. 7a–7c). IHC for Sox9, Cav-1, and AR showed that Sox9 (Figs. 7d–7f; black arrow), Cav-1 (Figs. 7g–7i; black arrow), and AR (Figs. 7j–7l; black arrow) were all expressed in the back skin, abdominal skin, and musk gland tissues of FMD. However, the AR staining intensity was lower in the back skin and abdominal skin. Sox9 and AR were mainly expressed in the nuclei of musk gland and skin tissues, while Cav-1 was localized on the cell membrane structure in the musk gland and skin tissues (Fig. 7). Based on visual observation, the Sox9, Cav-1, and AR staining intensity gradients were described (Table 3). The staining intensity was greater in the back skin and musk gland of FMD.

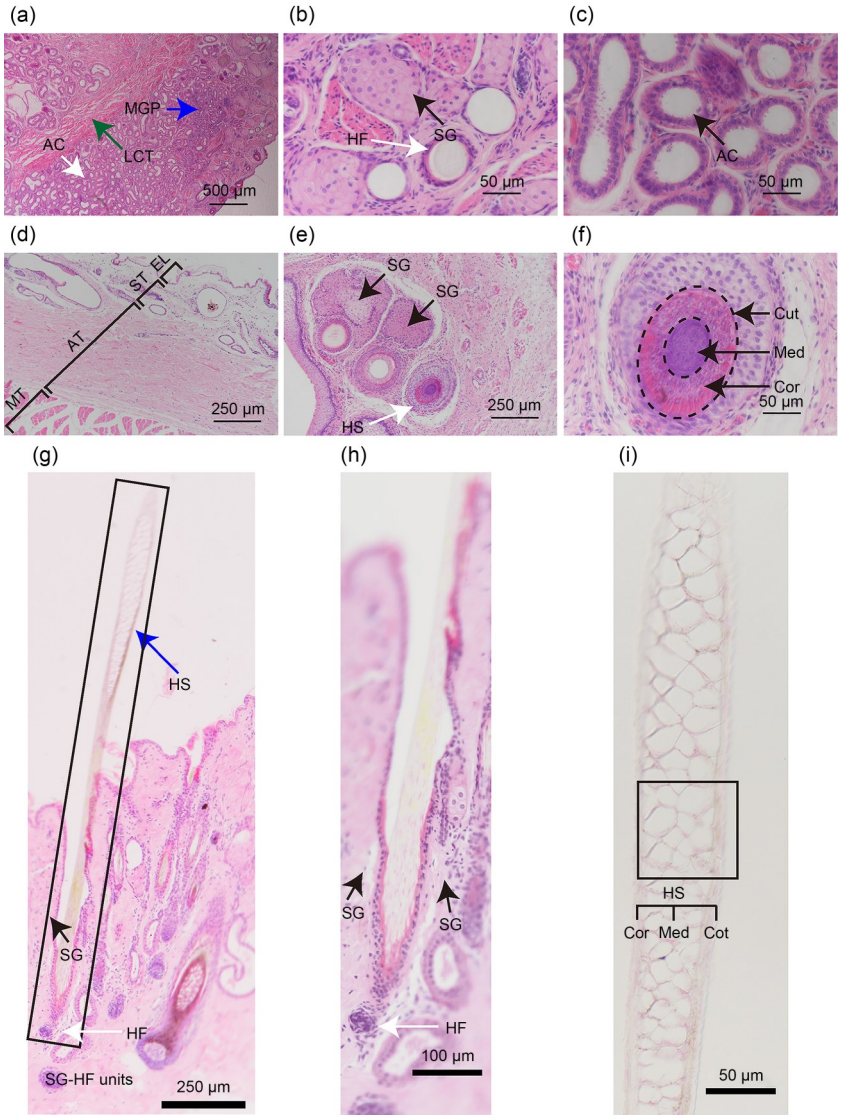

Fig. 6 Hematoxylin-eosin (HE) staining of the musk gland and skin tissues of 4-month-old forest musk deer (FMD). (a) General structure of the musk gland (4× objective lens). Green arrow, loose connective tissue (LCT); blue arrow, musk gland part (MGP); white arrow, acinar cavity (AC). (b) Musk gland skin junction (40× objective lens). The white arrow points to the hair follicle (HF), and the black arrow points to sebaceous gland (SG). (c) Part of musk gland (40× objective lens). The blank space represents the AC. (d) HE-stained sections of FMD skin tissue (10× objective lens): the figure shows the epidermal layer (EL), subcutaneous tissue (ST), adipose tissue (AT), and muscle tissue (MT). (e) The section of HE-stained FMD abdomen skin tissue. The black arrows indicate SG, and the white arrow points to hair shaft (HS) tissues in three different developmental stages. (f) Structure of the HS structure in FMD. The image shows the medulla (Med), cortex (Cor), and cuticle (Cut), which are pointed by black arrows. (g) The section of HE-stained FMD skin tissue. The rectangular box denotes a structural unit consisting of an SG and HF (SG-HF unit), including an SG (black arrow), HF (white arrow), and hair shaft (HS, blue arrow). (h) Microstructure of the HF (white arrow) and SG (black arrows). (i) The complete structure of the HS, including the Med, Cor, and Cut.

3.8 Validation of mRNA expression data using qRT-PCR

In order to verify *Sox9*, *Cav-1*, and *AR* mRNA expression, we performed qRT-PCR and validated the expression profiles of these three genes in the back skin, abdominal skin, and musk gland. The qRT-PCR results showed that *Sox9*, *Cav-1*, and *AR* were all expressed in the back skin, abdominal skin, and musk gland. *Sox9* gene expression was the highest in the musk gland and the lowest in the abdominal skin ($P<0.001$; Fig. 8a). Similarly, *Cav-1* expression was the highest in the musk gland tissue and the lowest in the

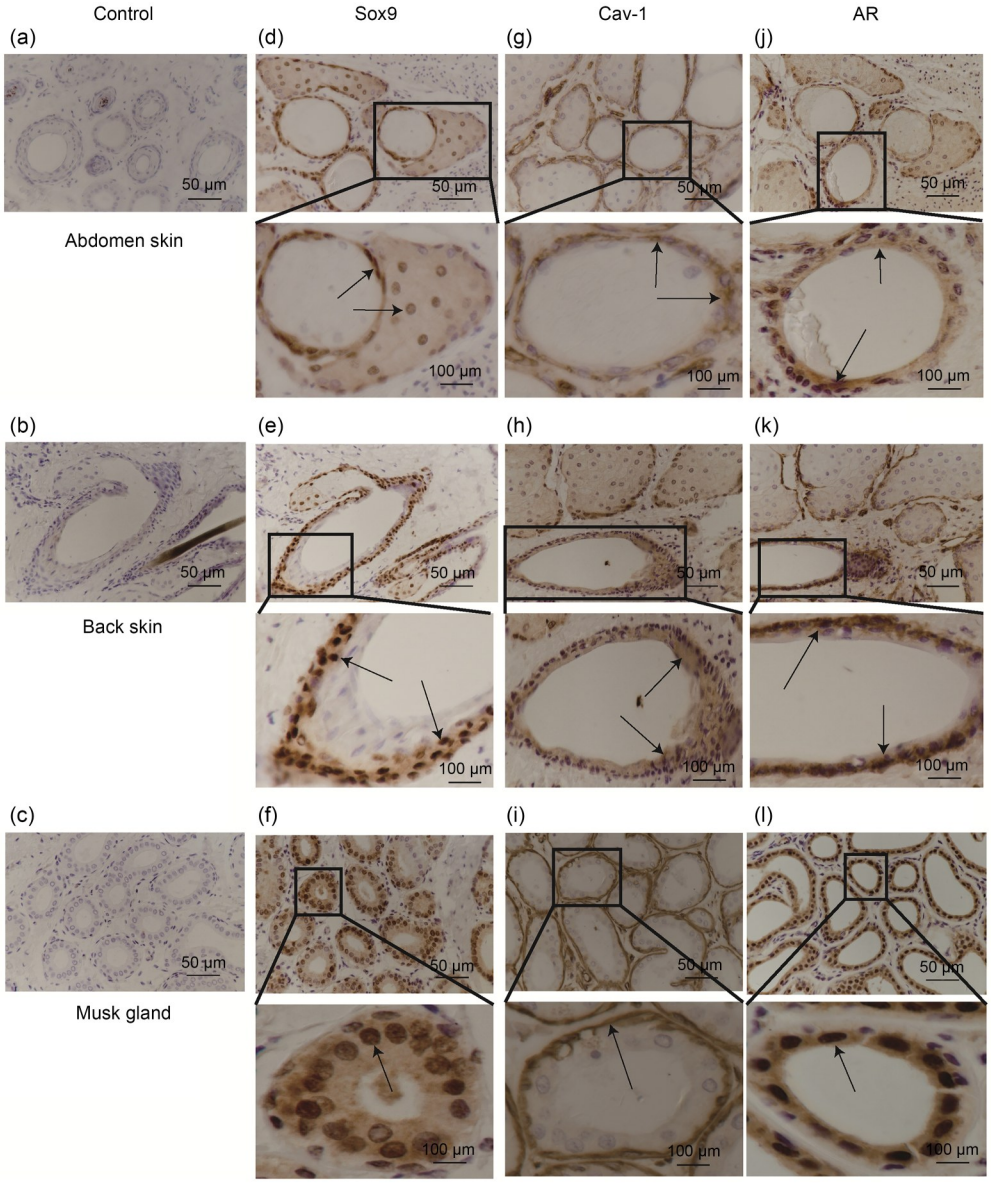

Fig. 7 Immunohistochemical results of sex-determining region Y box protein 9 (Sox9), Caveolin-1 (Cav-1), and androgen receptor (AR) in the abdominal skin, back skin, and musk gland tissues of 4-month-old male forest musk deer (FMD). (a–c) Negative control; (d–l) Expression and localization of sox9 (d–f), Cav-1 (g–i), and AR (j–l) proteins in the abdominal skin (d, g, j), back skin (e, h, k), and musk glands (f, i, l). Brown color indicates a positive signal for the corresponding protein (40× objective lens). The arrows indicate positive signals.

Table 3 Intensity of Sox9, Cav-1, and AR immunoreactivity based on visual inspection

Tissue	Protein		
	Sox9	Cav-1	AR
Abdomen skin	++	++	++
Back skin	+++	+++	+++
Musk gland	+++	++	+++

Immunoreactivity of tissue cell: moderate positive (++); strong positive (+++). AR: androgen receptor; Cav-1: Caveolin-1; Sox9: sex-determining region Y-box protein 9.

abdominal skin (P<0.001; Fig. 8b). In addition, *AR* expression was the highest in the musk gland, with no significant expression differences between the abdominal and back skin (P>0.05; Fig. 8c).

3.9 Protein expression of Sox9, Cav-1, and AR

With the aim to further evaluate the roles of Sox9, Cav-1, and AR in the development of the abdominal skin, back skin, and musk gland, protein expression

was detected using WB. The results are presented in Fig. 9. Sox9 was the most highly expressed in the musk gland and its expression was the lowest in the abdominal skin (Figs. 9a and 9b). Cav-1 and AR were

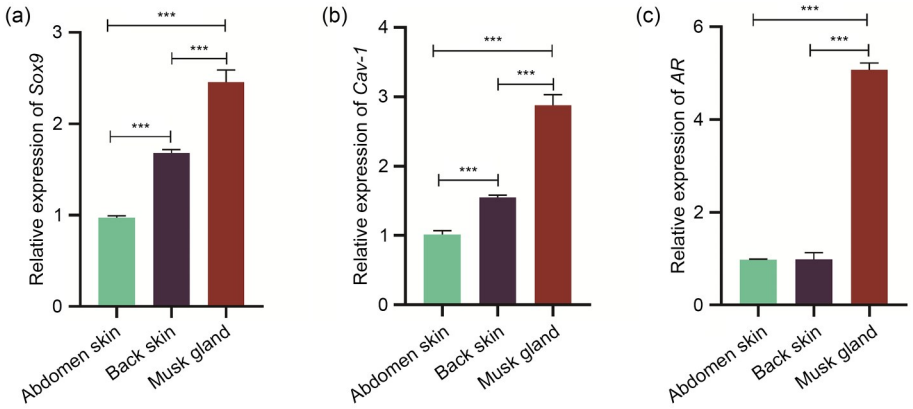

Fig. 8 mRNA expression of *Sox9* (a), *Cav-1* (b), and *AR* (c) in the abdominal skin, back skin, and musk gland detected by qRT-PCR. The mRNA expression levels of *Sox9*, *Cav-1*, and *AR* were normalized based on that of *GAPDH*. All data were obtained using three replicates, and the results are presented as mean±SD. The bar chart superscripts indicate significant differences (* $P<0.001$), and an unpaired *t*-test was used for analysis. *AR*: androgen receptor; *Cav-1*: Caveolin-1; *GAPDH*: glyceraldehyde-3-phosphate dehydrogenase; mRNA: messenger RNA; qRT-PCR: quantitative real-time polymerase chain reaction; SD: standard deviation; *Sox9*: sex-determining region Y box protein 9.**

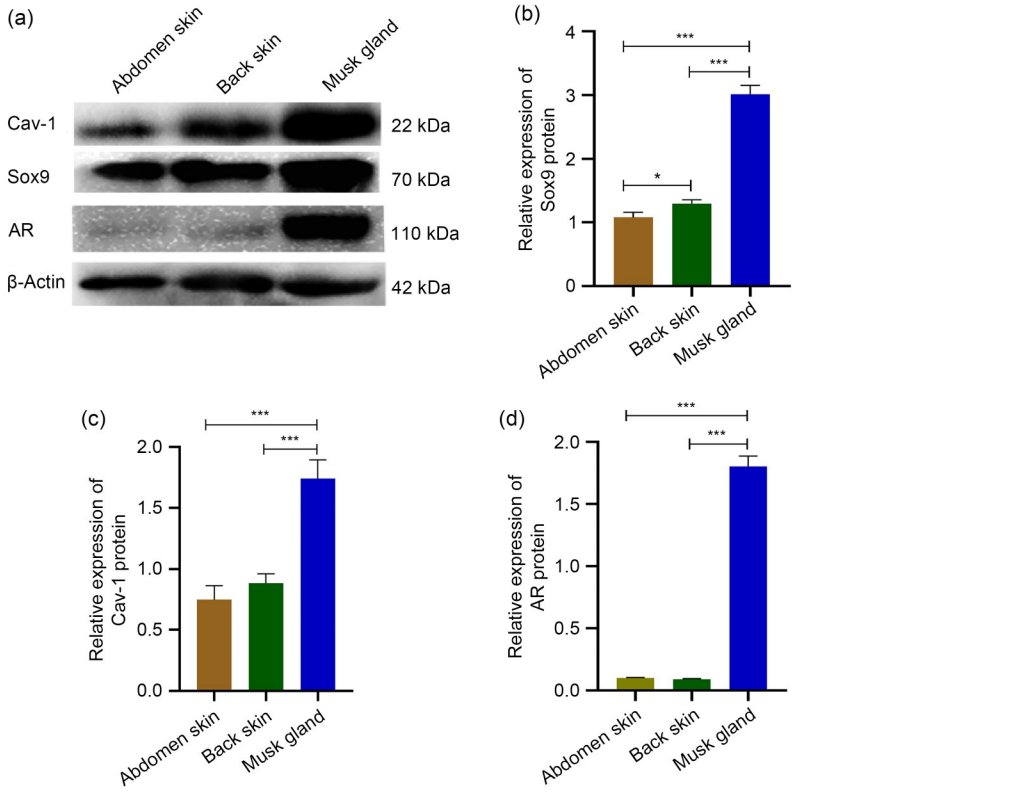

Fig. 9 Protein expression of Sox9, Cav-1, and AR in the abdominal skin, back skin, and musk gland tissues. (a) Western blot for detecting Sox9, Cav-1, and AR protein expression, with β-actin as the internal reference for protein detection. (b–d) Quantitative analyses of Sox9 (b), Cav-1 (c), and AR (d) proteins. All samples had three replicates, and the results are presented as mean±SD. The bar chart superscripts indicate significant differences (* $P<0.05$, *** $P<0.001$), and an unpaired *t*-test was used for analysis. AR: androgen receptor; Cav-1: Caveolin-1; SD: standard deviation; Sox9: sex-determining region Y box protein 9.

highly expressed in the musk gland (P<0.001) and the expression levels of these two proteins were similar between the abdominal skin and back skin (P>0.05; Figs. 9c and 9d).

4 Discussion

The musk secreted by FMD is an essential component of traditional Chinese medicine and perfume, and premature musk can be isolated from whole musk pods (Zhao et al., 2011; Picardo et al., 2015; Fan MY et al., 2018). As an extremely endangered species, FMD are on the China Red List, and their hunting has been banned (Paim et al., 2021; Su et al., 2022). Several studies have focused on live FMD, whereas we obtained highly precious FMD tissue samples that are still worth studying. Previous analysis of the chemical composition of musk found that it mainly contains fatty acids (71.55%), cholesterol (9.31%), esters, alcohols, and cyclic ketones (Fan MY et al., 2018; Zhang et al., 2021). It is thus of great significance to study musk glands and sebaceous glands that also produce a high amount of fatty acids.

By dissecting FMD tissues at different stages, we found that only adult male FMD have musk pods (Fig. S1b). The musk gland is a unique organ in FMD, and it can synthesize and secrete musk. Its development is synchronized with that of testes (Fuchs, 2016). In 4-month-old FMD, the musk gland cannot secrete musk, and a well-developed musk pod to store musk is still absent (Fig. S1a). As previously reported, adult male FMD can secrete musk during the breeding season, and the secretions enter the musk pod where this preliminary musk develops for about two months before reaching maturity (Picardo et al., 2015).

We analyzed the transcriptome data to gain a further and more comprehensive understanding of the relationship between skin tissues and musk glands. The Q20 of musk gland and skin tissues was more than 97%, and the Q30 was more than 93% (Table 2). This indicated the high precision of detection and high quality of sequencing data (Andrews, 2014). The unigene assembly results showed a high number of genes sized 200–300 bp and ≥2000 bp (Fig. 1). Previous studies have confirmed that these assembly results could be used for further analysis (Zhou et al., 2019). The Venn diagram analysis showed that the genes co-expressed in abdominal skin, back skin, and musk gland tissues accounted for 88.24% (29 771) of all total genes (Fig. 2). Metascape analysis demonstrated a strong correlation between the musk gland and the skin (Fig. 3). The genes and gene products could be classified and annotated into three GO annotation categories: biological process, molecular function, and cellular component (Fig. 4). KEGG pathway analysis for metabolic and synthetic activities in the musk gland and skin tissues was performed based on six categories: organismal systems, metabolism, human diseases, genetic information processing, environmental information processing, and cellular processes (Fig. 5).

The transcriptomic data revealed that the genes in the skin and musk glands of FMD were highly co-expressed, suggesting that these tissues had a strong correlation. We further studied this correlation from the perspective of histomorphology and carried out HE experiments. The skin and musk glands of FMD were found to be closely connected across the spatial dimension, and there were abundant sebaceous glands (Figs 6a, 6b, and 6d). Secretions from sebaceous glands in the skin and musk glands are crucial for development and homeostasis in FMD (Zhao et al., 2011; Fan ZX et al., 2018; Paim et al., 2021). Notably, some differences in histomorphology between skin tissues and musk glands were also observed. The skin exhibited a hair follicle structure and the musk gland had acinar cavities (Figs. 6c and 6e–6i). Sebaceous glands can form sebum units with hair follicles and interact with the skin surface via the hair canal, playing various roles in antibacterial functions, antioxidant activity, and pheromone communication (Storbeck et al., 2013). The musk gland secretions of FMD can enter the acinar cavity and collect in musk pods via gland ducts (Picardo et al., 2015).

The skin and musk glands of FMD are closely related in histomorphology and genetics, but tissue specificity is still maintained. Based on transcriptome data and previous related studies, we evaluate *Sox9*, *Cav-1*, and *AR* expression across different tissues in this study. *Sox9* has multiple functions in cell fate regulation, stem cell behavior, embryonic development, as well as acquired and congenital diseases (Jo et al., 2014). *Cav-1* plays a key role in regulating the proliferative capacity of epidermal stem cells, altering the proliferative capacity of epidermal stem cells and promoting wound healing (Yang et al., 2019). Androgens are primarily synthesized in the testes and have long been thought to act as male-sex steroids involved in

the acquisition of male secondary characteristics, and they mainly exert their functions via AR (Rege et al., 2013; Storbeck et al., 2013; Pretorius et al., 2016). IHC results showed that Sox9 and AR were localized in the nucleus and Cav-1 was expressed in the membrane in the abdominal skin, back skin, and musk gland tissues of FMD (Fig. 7). The qRT-PCR results showed that *Sox9*, *Cav-1*, and *AR* were highly expressed in the musk gland tissue (Fig. 8). Similarly, WB revealed that Sox9, Cav-1, and AR were highly expressed in the musk gland (Fig. 9). Sox9-positive cells are considered to be multipotent stem cells that can differentiate into both sebaceous gland cells and epithelial cells (Tamai et al., 2001; Jasmin et al., 2009; Shi et al., 2017). Cav-1 regulates cell proliferation (Tamai et al., 2001; Faggi et al., 2015). The number of cells expressing stem cell markers was found to be elevated in several organs, including the intestine, mammary glands, and brain of Cav-1 null mice (Li et al., 2005; Sotgia et al., 2005; Jasmin et al., 2009). In the classical testosterone signaling pathway, androgen exerts its genomic effect through AR. Testosterone is mainly produced by the testes, and the development of the musk gland is synchronized with that of the testes (Quigley et al., 1995). Previous studies have shown that both Sox9 and Cav-1 can interact with AR, and androgens play an important regulatory role in the secretion of these from the musk gland (Barrault et al., 2015; Duarte et al., 2019). Together, these results indicate that Sox9, Cav-1, and AR may play important roles in the development of skin and musk glands in FMD.

In summary, this study compared and analyzed the tissue morphology, gene expression, and protein expression profiles of abdominal skin, back skin, and musk glands of FMD through HE, IHC, WB, qRT-PCR, and RNA-seq. The proportion of genes co-expressed across the abdominal skin, back skin, and musk glands was as high as 88.24%, and the highly expressed genes were mainly enriched in adipocytes, bronchial epithelial cells, and skin tissue, implying common genetic and tissue origins across these three structures. The key regulatory gene *Sox9*, the *AR*, and the signal transduction hub gene *Cav-1* were expressed in the abdominal skin, back skin, and musk gland. Overall, these data suggested that the musk gland and skin tissues have a strong relationship, that is, the musk gland is likely derived from the skin (Fig. 10).

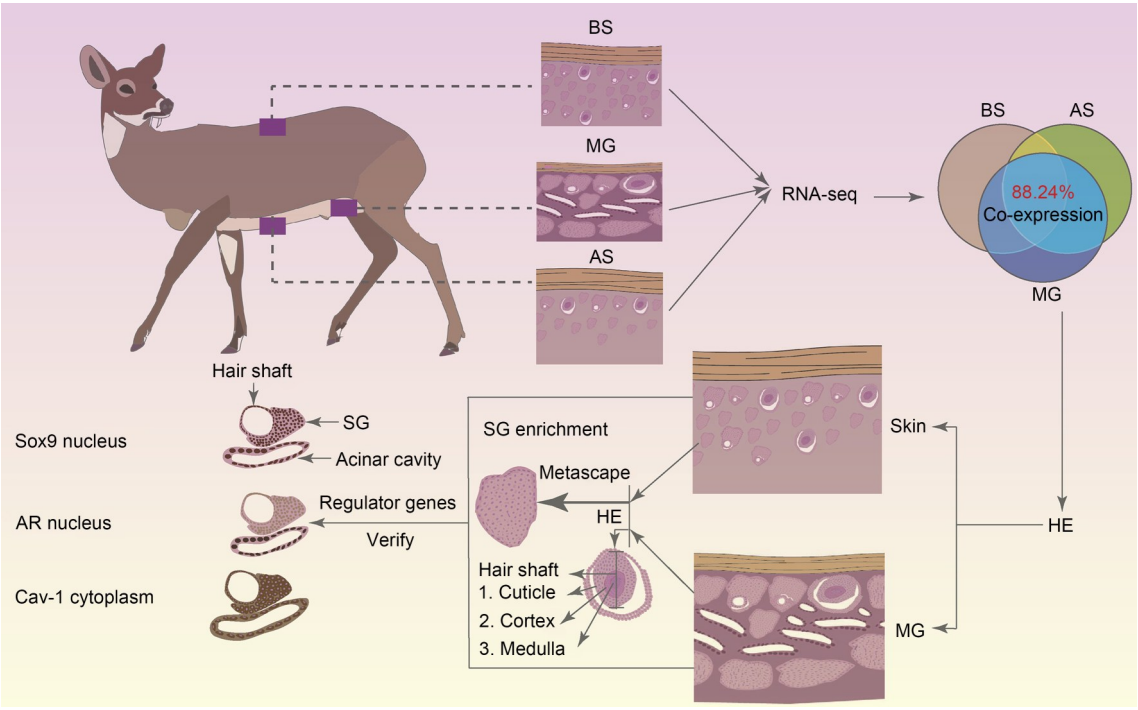

Fig. 10 Schematic representation of the relationships among the back skin, abdominal skin, and musk gland of forest musk deer (FMD) at the tissue, cell, and gene levels. AR: androgen receptor; AS: abdominal skin; BS: back skin; Cav-1: Caveolin-1; HE: hematoxylin-eosin; MG: musk gland; RNA-seq: RNA sequencing; SG: sebaceous gland; Sox9: sex-determining region Y-box protein 9.

Data availability statement

All data will be available on request.

Acknowledgments

This work was supported by the Key Sci-Tech Project of Shaanxi Province (No. 2018ZDXM-NY-034) and the Innovation Capability Support Program of Shaanxi Province (No. 2018-TD-021), China. We acknowledge the support by the Northwest A&F University and the reproductive biology and cell engineering team. We acknowledge Mr. Xuezhe ZHANG at the Shaanxi Baosen Musk Deer Industry Co., Ltd. (Shaanxi, China) for providing experimental animals.

Author contributions

Wuzi DONG and Fangxia YANG put forward the design. Long LI is responsible for data statistics, manuscript writing, and the completion of related experiments. Heran CAO is responsible for relevant experiments and articles review. Yuxuan MA, Jinmeng YANG, Yang WANG, Huihui GAO, Tianqi JIN, Zhenpeng LI, Yining CHEN, Tianhao YANG, Yalong DENG, and Chao ZHU are responsible for sample collection and RNA extraction, and performed relevant experiments. Wuzi DONG proofread the final manuscript. Finally, all authors have read and agreed with the eventual manuscript, and therefore, have full access to all the data in the study and take responsibility for the integrity and security of the data.

Compliance with ethics guidelines

Long LI, Heran CAO, Jinmeng YANG, Tianqi JIN, Yuxuan MA, Yang WANG, Zhenpeng LI, Yining CHEN, Huihui GAO, Chao ZHU, Tianhao YANG, Yalong DENG, Fangxia YANG, and Wuzi DONG declare they have no conflict of interest.

All experimental animal procedures were reviewed and approved by the Ethical Committee of Northwest A&F University (No. AAEWV-NWSUAF-DK2021050).

References

Andrews S, 2014. FastQC a quality control tool for high throughput sequence data. https://www.bioinformatics.babraham.ac.uk/projects/fastqc

Barrault C, Garnier J, Pedretti N, et al., 2015. Androgens induce sebaceous differentiation in sebocyte cells expressing a stable functional androgen receptor. *J Steroid Biochem Mol Biol*, 152:34-44. https://doi.org/10.1016/j.jsbmb.2015.04.005

Bastiani M, Liu LB, Hill MM, et al., 2009. MURC/Cavin-4 and cavin family members form tissue-specific caveolar complexes. *J Cell Biol*, 185(7):1259-1273. https://doi.org/10.1083/jcb.200903053

Bennett N, Hooper JD, Lee CS, et al., 2009. Androgen receptor and caveolin-1 in prostate cancer. *IUBMB Life*, 61(10): 961-970. https://doi.org/10.1002/iub.244

Biggs LC, Mikkola ML, 2014. Early inductive events in ectodermal appendage morphogenesis. *Semin Cell Dev Biol*, 25-26:11-21. https://doi.org/10.1016/j.semcdb.2014.01.007

Boscher C, Nabi IR, 2012. CAVEOLIN-1: role in cell signaling. *In*: Jasmin JF, Frank PG, Lisanti MP (Eds.), Caveolins and Caveolae. Advances in Experimental Medicine and Biology, Vol. 729. Springer, New York, p.29-50. https://doi.org/10.1007/978-1-4614-1222-9_3

Buchfink B, Xie C, Huson DH, 2015. Fast and sensitive protein alignment using DIAMOND. *Nat Methods*, 12(1):59-60. https://doi.org/10.1038/nmeth.3176

Chen M, Jie H, Xu ZX, et al., 2018. Isolation, primary culture, and morphological characterization of gland epithelium from forest musk deer (*Moschus berezovskii*). *In Vitro Cell Dev Biol Anim*, 54(8):545-548. https://doi.org/10.1007/s11626-018-0268-0

Codenotti S, Vezzoli M, Poliani PL, et al., 2016. Caveolin-1, Caveolin-2 and Cavin-1 are strong predictors of adipogenic differentiation in human tumors and cell lines of liposarcoma. *Eur J Cell Biol*, 95(8):252-264. https://doi.org/10.1016/j.ejcb.2016.04.005

Downie MMT, Guy R, Kealey T, 2004. Advances in sebaceous gland research: potential new approaches to acne management. *Int J Cosmet Sci*, 26(6):291-311. https://doi.org/10.1111/j.1467-2494.2004.00238.x

Duarte MF, Luis C, Baylina P, et al., 2019. Clinical and metabolic implications of obesity in prostate cancer: is testosterone a missing link? *Aging Male*, 22(4):228-240. https://doi.org/10.1080/13685538.2018.1519695

Faggi F, Chiarelli N, Colombi M, et al., 2015. Cavin-1 and Caveolin-1 are both required to support cell proliferation, migration and anchorage-independent cell growth in rhabdomyosarcoma. *Lab Invest*, 95(6):585-602. https://doi.org/10.1038/labinvest.2015.45

Fan MY, Zhang MS, Shi MH, et al., 2018. Sex hormones play roles in determining musk composition during the early stages of musk secretion by musk deer (*Moschus berezovskii*). *Endocr J*, 65(11):1111-1120. https://doi.org/10.1507/endocrj.EJ18-0211

Fan ZX, Li WJ, Jin JZ, et al., 2018. The draft genome sequence of forest musk deer (*Moschus berezovskii*). *Gigascience*, 7(4):giy038. https://doi.org/10.1093/gigascience/giy038

Fridolfsson HN, Roth DM, Insel PA, et al., 2014. Regulation of intracellular signaling and function by caveolin. *FASEB J*, 28(9):3823-3831. https://doi.org/10.1096/fj.14-252320

Fu Y, Moore XL, Lee MKS, et al., 2012. Caveolin-1 plays a critical role in the differentiation of monocytes into macrophages. *Arterioscler Thromb Vasc Biol*, 32(9):e117-e125. https://doi.org/10.1161/atvbaha.112.254151

Fuchs E, 2016. Epithelial skin biology: three decades of developmental biology, a hundred questions answered and a thousand new ones to address. *Curr Top Dev Biol*, 116: 357-374. https://doi.org/10.1016/bs.ctdb.2015.11.033

Haas BJ, Papanicolaou A, Yassour M, et al., 2013. *De novo* transcript sequence reconstruction from RNA-seq using the Trinity platform for reference generation and analysis.

Nat Protoc, 8(8):1494-1512. https://doi.org/10.1038/nprot.2013.084

Huang SY, Huang GJ, Wu HC, et al., 2018. *Ganoderma tsugae* inhibits the SREBP-1/AR axis leading to suppression of cell growth and activation of apoptosis in prostate cancer cells. *Molecules*, 23(10):2539. https://doi.org/10.3390/molecules23102539

Jasmin JF, Yang M, Iacovitti L, et al., 2009. Genetic ablation of caveolin-1 increases neural stem cell proliferation in the subventricular zone (SVZ) of the adult mouse brain. *Cell Cycle*, 8(23):3978-3983. https://doi.org/10.4161/cc.8.23.10206

Jiang YL, Han XY, Feng NN, et al., 2022. Androgen plays an important role in regulating the synthesis of pheromone in the scent gland of muskrat. *J Steroid Biochem Mol Biol*, 217:106026. https://doi.org/10.1016/j.jsbmb.2021.106026

Jo A, Denduluri S, Zhang BS, et al., 2014. The versatile functions of Sox9 in development, stem cells, and human diseases. *Genes Dis*, 1(2):149-161. https://doi.org/10.1016/j.gendis.2014.09.004

Khurana N, Sikka SC, 2019. Interplay between SOX9, Wnt/β-catenin and androgen receptor signaling in castration-resistant prostate cancer. *Int J Mol Sci*, 20(9):2066. https://doi.org/10.3390/ijms20092066

Li JW, Hassan GS, Williams TM, et al., 2005. Loss of caveolin-1 causes the hyper-proliferation of intestinal crypt stem cells, with increased sensitivity to whole body γ-radiation. *Cell Cycle*, 4(12):1817-1825. https://doi.org/10.4161/cc.4.12.2199

Li RQ, Li YR, Kristiansen K, et al., 2008. SOAP: short oligonucleotide alignment program. *Bioinformatics*, 24(5):713-714. https://doi.org/10.1093/bioinformatics/btn025

Lv SQ, Lei ZX, Yan G, et al., 2022. Chemical compositions and pharmacological activities of natural musk (*Moschus*) and artificial musk: a review. *J Ethnopharmacol*, 284:114799. https://doi.org/10.1016/j.jep.2021.114799

Paim FP, Carretero-Pinzón X, Guzmán-Caro DC, et al., 2021. The IUCN Red List of threatened species. https://www.iucnredlist.org

Picardo M, Mastrofrancesco A, Bíró T, 2015. Sebaceous gland–a major player in skin homoeostasis. *Exp Dermatol*, 24(7):485-486. https://doi.org/10.1111/exd.12720

Pretorius E, Africander DJ, Vlok M, et al., 2016. 11-Ketotestosterone and 11-ketodihydrotestosterone in castration resistant prostate cancer: potent androgens which can no longer be ignored. *PLoS ONE*, 11(7):e0159867. https://doi.org/10.1371/journal.pone.0159867

Quigley CA, de Bellis A, Marschke KB, et al., 1995. Androgen receptor defects: historical, clinical, and molecular perspectives. *Endocr Rev*, 16(3):271-321. https://doi.org/10.1210/edrv-16-3-271

Rege J, Nakamura Y, Satoh F, et al., 2013. Liquid chromatography-tandem mass spectrometry analysis of human adrenal vein 19-carbon steroids before and after ACTH stimulation. *J Clin Endocrinol Metab*, 98(3):1182-1188. https://doi.org/10.1210/jc.2012-2912

Saga K, 2002. Structure and function of human sweat glands studied with histochemistry and cytochemistry. *Prog Histochem Cytochem*, 37(4):323-386. https://doi.org/10.1016/s0079-6336(02)80005-5

Schneider MR, Paus R, 2010. Sebocytes, multifaceted epithelial cells: lipid production and holocrine secretion. *Int J Biochem Cell Biol*, 42(2):181-185. https://doi.org/10.1016/j.biocel.2009.11.017

Shakhova O, Cheng P, Mishra PJ, et al., 2015. Antagonistic cross-regulation between Sox9 and Sox10 controls an anti-tumorigenic program in melanoma. *PLoS Genet*, 11(1):e1004877. https://doi.org/10.1371/journal.pgen.1004877

Shi G, Sohn KC, Li ZJ, et al., 2013. Expression and functional role of Sox9 in human epidermal keratinocytes. *PLoS ONE*, 8(1):e54355. https://doi.org/10.1371/journal.pone.0054355

Shi G, Wang TT, Quan JH, et al., 2017. Sox9 facilitates proliferation, differentiation and lipogenesis in primary cultured human sebocytes. *J Dermatol Sci*, 85(1):44-50. https://doi.org/10.1016/j.jdermsci.2016.10.005

Shirasu M, Ito S, Itoigawa A, et al., 2020. Key male glandular odorants attracting female ring-tailed lemurs. *Curr Biol*, 30(11):2131-2138.e4. https://doi.org/10.1016/j.cub.2020.03.037

Slessor KN, Winston ML, le Conte Y, 2005. Pheromone communication in the honeybee (*Apis mellifera* L.). *J Chem Ecol*, 31(11):2731-2745. https://doi.org/10.1007/s10886-005-7623-9

Smith KR, Thiboutot DM, 2008. *Thematic review series: Skin Lipids*. Sebaceous gland lipids: friend or foe? *J Lipid Res*, 49(2):271-281. https://doi.org/10.1194/jlr.R700015-JLR200

Sokolov VE, Kagan MZ, Vasilieva VS, et al., 1987. Musk deer (*Moschus moschiferus*): reinvestigation of main lipid components from preputial gland secretion. *J Chem Ecol*, 13(1):71-83. https://doi.org/10.1007/bf01020352

Sotgia F, Williams TM, Cohen AW, et al., 2005. Caveolin-1-deficient mice have an increased mammary stem cell population with upregulation of Wnt/β-catenin signaling. *Cell Cycle*, 4(12):1808-1816. https://doi.org/10.4161/cc.4.12.2198

Sotiropoulou PA, Blanpain C, 2012. Development and homeostasis of the skin epidermis. *Cold Spring Harb Perspect Biol*, 4(7):a008383. https://doi.org/10.1101/cshperspect.a008383

Storbeck KH, Bloem LM, Africander D, et al., 2013. 11β-Hydroxydihydrotestosterone and 11-ketodihydrotestosterone, novel C19 steroids with androgenic activity: a putative role in castration resistant prostate cancer? *Mol Cell Endocrinol*, 377(1-2):135-146. https://doi.org/10.1016/j.mce.2013.07.006

Su RN, Dalai M, Luvsantseren B, et al., 2022. Comparative study of the function and structure of the gut microbiota in Siberian musk deer and Forest musk deer. *Appl Microbiol*

Biotechnol, 106(19-20):6799-6817. https://doi.org/10.1007/s00253-022-12158-9

Tamai O, Oka N, Kikuchi T, et al., 2001. Caveolae in mesangial cells and caveolin expression in mesangial proliferative glomerulonephritis. *Kidney Int*, 59(2):471-480. https://doi.org/10.1046/j.1523-1755.2001.059002471.x

Thody AJ, Shuster S, 1989. Control and function of sebaceous glands. *Physiol Rev*, 69(2):383-416. https://doi.org/10.1152/physrev.1989.69.2.383

Varendi H, Porter RH, 2001. Breast odour as the only maternal stimulus elicits crawling towards the odour source. *Acta Paediatr*, 90(4):372-375.

Vidal VPI, Ortonne N, Schedl A, 2008. SOX9 expression is a general marker of basal cell carcinoma and adnexal-related neoplasms. *J Cutan Pathol*, 35(4):373-379. https://doi.org/10.1111/j.1600-0560.2007.00815.x

Yang JM, Peng GF, Shu F, et al., 2021. Characteristics of steroidogenesis-related factors in the musk gland of Chinese forest musk deer (*Moschus berezovskii*). *J Steroid Biochem Mol Biol*, 212:105916. https://doi.org/10.1016/j.jsbmb.2021.105916

Yang RH, Wang JR, Zhou ZH, et al., 2019. Role of caveolin-1 in epidermal stem cells during burn wound healing in rats. *Dev Biol*, 445(2):271-279. https://doi.org/10.1016/j.ydbio.2018.11.015

Zhang TX, Zhang MS, Shi MH, et al., 2021. Musk secretion in muskrats (*Ondatra zibethicus* L.): association with lipid and cholesterol metabolism-related pathways. *Biocell*, 45(2):281-306. https://doi.org/10.32604/biocell.2021.010277

Zhao KL, Liu Y, Zhang XY, et al., 2011. Detection and characterization of antibiotic-resistance genes in *Arcanobacterium pyogenes* strains from abscesses of forest musk deer. *J Med Microbiol*, 60(12):1820-1826. https://doi.org/10.1099/jmm.0.033332-0

Zhou YY, Zhou B, Pache L, et al., 2019. Metascape provides a biologist-oriented resource for the analysis of systems-level datasets. *Nat Commun*, 10:1523. https://doi.org/10.1038/s41467-019-09234-6

Zouboulis CC, Baron JM, Böhm M, et al., 2008. Frontiers in sebaceous gland biology and pathology. *Exp Dermatol*, 17(6):542-551. https://doi.org/10.1111/j.1600-0625.2008.00725.x

Supplementary information

Figs. S1–S4